Beam-Transport System of KEKB

M. Kikuchi, T. Honda, N. Iida, K. Kanazawa, T. Kubo,
T. Mimashi, H. Nakayama, Y. Sakamoto, K.Satoh,
Y. Takeuchi, M. Yoshida and M. Yoshioka

KEK, National High Energy Accelerator Research Organization, 1-1 Oho, Tsukuba-shi, Ibaraki-ken, 305-0801 Japan

Abstract

The transport lines of the KEKB for positrons and electrons convey the beams separately from the injector linac to the KEKB rings. The length is about 500 m for each line. In order to make the maximum use of the existing tunnels and also to avoid interference with the AR, the beam lines took a serpentine course, resulting in a rather large curvature in the arcs. The consequences were a large number of bends in the arcs with high fields and also a large dispersion function and, thus, a large R_{56} component. The latter issue is crucial for the KEKB rings, since it results in a longer bunch length at injection. We adopted a special optics that reduces the R_{56} coefficient sufficiently. We have developed novel water-cooled ceramic chambers for kickers, eddy-current type septum magnets for injection, and a beam-abort system for the rings. The present paper describes the design and current status of the beam lines, the injection system, and the beam-abort system.

Key words: beam, transport, KEKB, abort, kicker, septum, ceramic, bpm, wire

1 Introduction

KEKB is an asymmetric double-ring collider of 3.5-GeV positrons (LER) and 8-GeV electrons (HER), filled with current of 2.6 A for LER and 1.1 A for HER in the design. The beam-transport (BT) lines transfer the positron and electron beams separately from the injector linac to the rings, each having a length of about 500 m. The maximum repetition of the linac is 50 Hz. We describe the beam transport and the injection system in sections 2 and 3. The KEKB rings have a beam-abort system to protect the physics detector and accelerator components. It ejects beams to the dump in a single turn. We describe the beam-abort system in section 4.

2 Beam Transport Lines

The design specifications of the beam parameters are given in Table 1. The

Table 1
Beam parameters

	positrons	electrons
Energy	3.5 GeV	8.0 GeV
Emittance (Linac)	2.2×10^{-7} m	1.6×10^{-8} m
Acceptance (BT)	3.6×10^{-7} m	4.6×10^{-7} m
Energy spread (Linac)	1.25×10^{-3}	1.25×10^{-3}
Energy acceptance (BT)	2.5×10^{-3}	2.5×10^{-3}
Bunch length (Linac)	3.4 mm	1.7 mm
Bunch length (BT:end)	7.0 mm	7.1 mm

energy spread of the positron beam at the end of the linac is 2.5×10^{-3} and is compressed to one half by the energy compression system (ECS) at the most upstream part of the BT line.

2.1 Layout of the Beam Lines

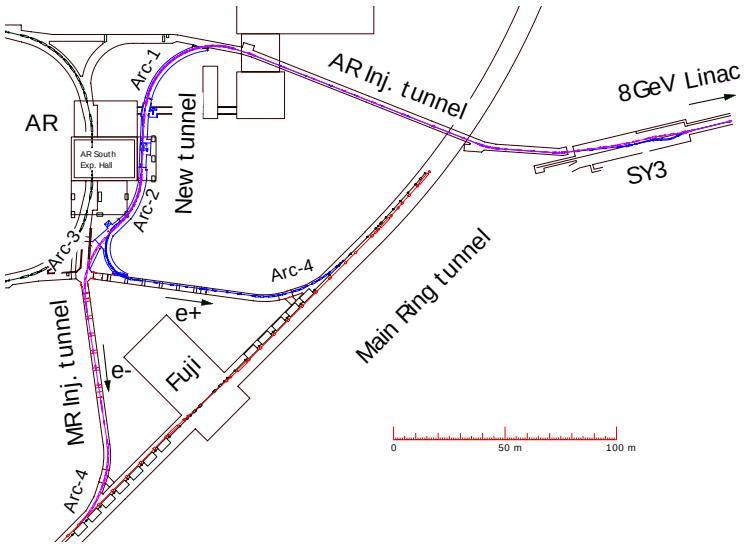

Fig. 1. Layout of the beam lines.

The layout of the beam lines, shown in Fig. 1, was decided under the guideline that maximum use should be made of the existing AR- and MR-injection tunnel and as large a separation as possible must be made from the Accumulator

Ring(AR), which had been planed to serve as a photon source. From these external conditions, a new tunnel was built that connects the AR-injection tunnel and the MR-injection tunnel, bypassing the South Hall of the AR. Another important design consideration was operational simplicity. If a single beam line is used for both electrons and positrons having different energies, the need to re-adjust the magnet excitations or to switch their polarities tends to create various operational complications. Thus, two beam lines have been implemented separately for the electrons and positrons. The beam lines have no common magnets nor common magnet power supplies, except for the first magnet that separates the two beams from the linac.

The positron and electron beams are separated at the exit of the linac and guided to each line. Fig. 2 shows a part of beam lines in an area called SY3, which is immediately downstream of the the linac exit before reaching the AR injection tunnel. Upstream of the SY3, an energy compression system was

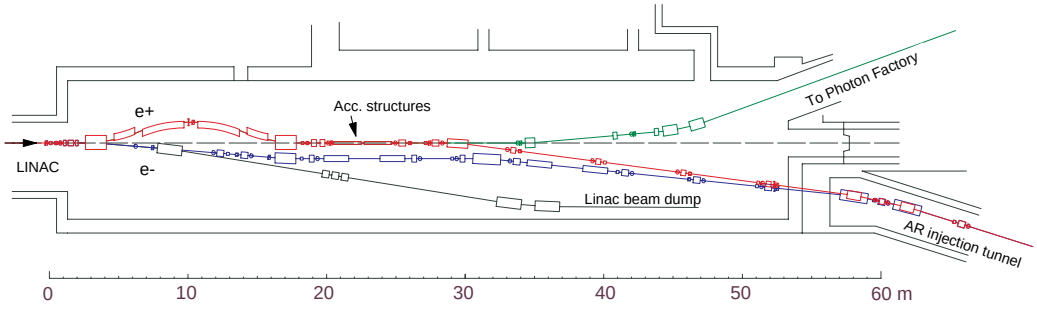

Fig. 2. Layout of the Beam Switch Yard (SY3)

implemented. Its purpose is to reduce the energy spread of the positrons from the linac by a factor of 1/2, and to relax the the energy acceptance of the beam-transport line as well as that of LER. The ECS consists of a chicane, composed of six 1.5 T bends, and two 2 m-long S-band accelerating structures. The electrons are simply separated from the positrons by the first bend of the ECS. Since the AR injection tunnel does not have sufficient space, 3 m wide and 2.5 m high, the lines were stacked vertically, with the positron line on top of the electron line.

In the middle of the new tunnel, immediately after the first arc (Arc-1), the two lines are separated horizontally. The elevation of the positron line is reduced in the subsequent straight section to meet the MR injection tunnel at an appropriate point in the middle of the MR injection line: the vertical separation of two beams is 0.9 m in the Arc-2 and Arc-3. After passing the downward slopes only minor modifications to the injection lines are required, since the injection points to the KEKB rings are at nearly the same positions as those of the TRISTAN MR. Fig. 3 shows a typical view at the Arc-1 of the new BT tunnel.

Fig. 3. Typical view from upstream at Arc-1.

2.2 Optics

Tight constraints on the geometric conditions led to a large curvature of the beam lines in the new tunnel. A simple repeat of identical FODO cell would produce a large dispersion function in the arcs, which would result, combined with the small bend radius, a large R_{56} component. Here, R_{56} refers to the (5,6) component of the transfer matrix, *i.e.*, the path-length dependence on the momentum. A larger R_{56} generates a longer bunch length at the end of BT due to drift in the longitudinal phase space. A beam with a large bunch length, correlated with momentum, induces a large quadrupole synchrotron oscillation. We adopted special optics that reduces R_{56}: the optics around the three arcs in the new tunnel was arranged such that the dispersion function was reversed in the middle of the arc *or* upstream of one arc generated negative dispersion downstream of the arc so that in total R_{56} was decreased. This approach demands, however, that almost all quads are powered independently. In the present optics, the bunch length is still dominated by the longitudinal drift effects, as shown in the Table 1. In this optics the largest energy amplitude of the induced bunch oscillation immediately after injection is much smaller than the longitudinal acceptance of the rings in the worst case (0.5 %). Fig. 4 shows the optics function of the beam lines. The dispersion function is kept relatively small and closed within each region. The parameter R_{56} is -4.9 m for positrons and -5.5 m for electrons at the end of the beam lines.

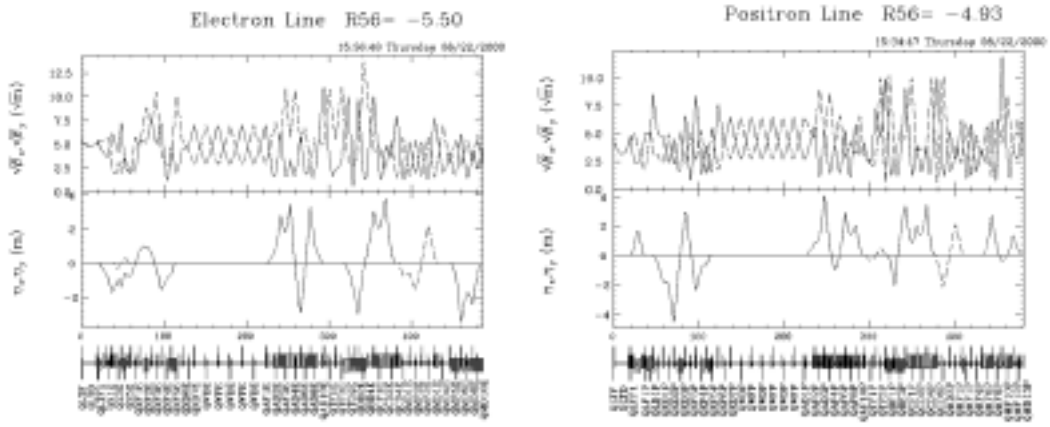

Fig. 4. Optics functions: In order to maintain R_{56} to be as small as possible, the dispersion function is reversed in the middle of the arcs.

2.3 Beam Halo Collimation

Beam halo collimation is vitally important to protect the fragile detectors of the Belle from lost particles. Although the KEKB rings have their own masks, it is preferable to cut the tail part of the beams before injection. The collimation system is also necessary to reduce the beam loss in the undesirable part of the transport lines. We installed 12 pairs of collimators; among them, two are for collimating the energy-tail of positrons and the others are for collimating the emittance-tail for both beams. Two sections, SY3 and the Arc-1, are equipped with energy collimators. The dispersion function was made to be as large as 4 m at both locations while keeping the beta function as small as possible to obtain a higher energy resolution. In the current operation, the energy collimation in the SY3 has been effective to suppress the radiation level, while both collimators have had no distinct effect in reducing the beam backgrounds of Belle.

2.4 Operation Status

In the commissioning we first made a relative calibration of the quad strength to the bend strength. This procedure was necessary because we had made field measurements using different coils for quads and bends and had not made a calibration between coils. An unknown factor was thus common to all quads. We measured the leakage of the dispersion function downstream of one arc, where the dispersion is zero in design, as a function of the common factor for the quads included in that arc. After the calibration, the dispersion function in all of the arcs of the beam lines was found to be locally closed. Secondly, we performed optics matching between the linac and the BT using wire scanners. This was very effective, especially in recovery of the linac after a long shut-

down. Since we could not make an intensity calibration between the BPMs the transmission efficiency has an ambiguous factor. A precise calibration was difficult because the cable length of the BPMs differs significantly. The injection efficiency is 100% at maximum and is strongly dependent on the aperture condition of rings, defined with masks *etc.*

2.5 Instrumentation

2.5.1 Beam Position Monitor

Both the positron and electron lines are equipped with beam-position monitors(BPM) of 61 and 56, respectively. The BPMs are attached to every quadrupole magnet. A BPM comprises four strip-line type pickup electrodes, shown in Fig. 5. The length of the electrode is 175 mm. Each electrode spans 45° to the beam center and forms a part of a cylinder whose diameter is 52 mm, slightly wider than the standard aperture, 49 mm, of the beam chamber in the transport line. The characteristic impedance of the electrode is matched 50 Ω. In order to avoid any adverse effect of synchrotron light, electrodes are placed such that the synchrotron light escapes through the space between two electrodes. The mechanical precision for the assembly of the electrodes was controlled within ±0.1 mm.

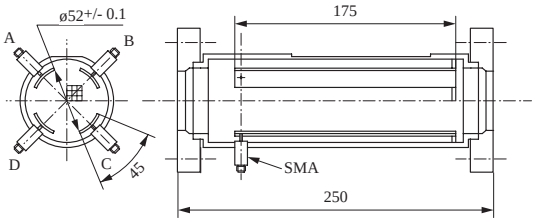

Fig. 5. Strip-line electrodes for the BPM

Single-pass measurements of BPM signals utilizing a waveform digitizer or a digital oscilloscope have been used in the electron accelerators of KEK[2,3]. Fig. 6 shows a schematic diagram of signal combination in the present system. In order to save the amount of cable, the signals of four BPMs are combined in a single cable in the tunnel, and these four combined signals are, moreover, combined in a single cable in the local control room; eventually, 16 signals are combined in a single cable. The peak-to-peak amplitude of the BPM signal is detected with a VXI-based waveform analyzer. A coaxial switch selects the signal from the two beam lines; thus, a single channel of the waveform analyzer covers 32 BPMs. We used a 8D-class coaxial cable having a corrugated copper tube as an outer conductor. The transmission length ranges from 100 m to 300 m. The total cable length used for the BPM system amounts to 50 km.

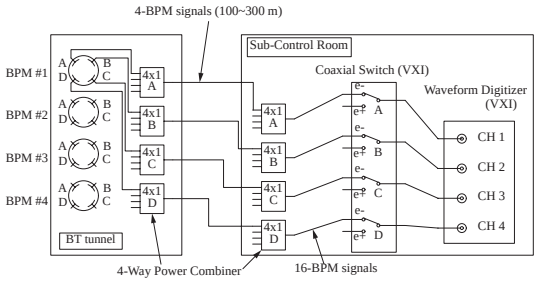

Fig. 6. Schematic diagram of the BPM signal combination.

The maximum sampling speed of the digitizer is 5 GS/s and the voltage resolution is 8 bits. Since the fundamental frequency of the signal is 1 GHz, which is comparable to an input bandwidth of 1 GHz, we have limited it to 250 MHz with a low-pass filter. The peak-to-peak value is thus more precisely detected with more immunity to the timing jitter. The power combiner has a bandwidth of 1 GHz. The total insertion loss is about 7 dB.

In the present system, the four signals from one BPM are recorded with different channels of the waveform digitizer. Differences of a few meters in the cable lengths have no effect on the precision. Differences in the transmission loss among the four electrodes, however, cause an offset of the BPM center. The transmission loss, including cables and the power combiners, were measured at two frequencies of 200 MHz and 500 MHz at a resolution of 0.1 dB. The measured amplitudes of the beam signals were corrected based on the data of the transmission loss. An error of 0.1 dB in the signal amplitude approximately corresponds to an error of 0.1 mm in the beam-position offset. During operation, the bunch charge of electrons (positrons) was 2 nC (0.6 nC). The observed amplitude of the beam signal was from 0.2 V to 2 V, depending on the cable length, when the bunch charge was 0.6 nC. A position resolution of 100 μm has been achieved, which is dominated by the digitizing resolution of the waveform analyzer.

The beam orbit of the beam transport line is continuously monitored during injection. Fig. 7 shows an example of the positron orbit along with the whole beam transport line. A typical cycle of data acquisition is 1 to 2 seconds. The beam intensity is plotted in the third row of the figure. The beam intensity was estimated from summing the four electrode signals.

2.5.2 Wire Scanner etc.

In order to make matching the optics between the linac and BT, four wire scanners have been installed at the long straight section in each beam line in between SY3 and Arc-1, where the dispersion function is zero in design. Another wire scanner was also installed at the entrance of the Arc-4 section in each line for measuring the residual mismatch and for its correction prior to

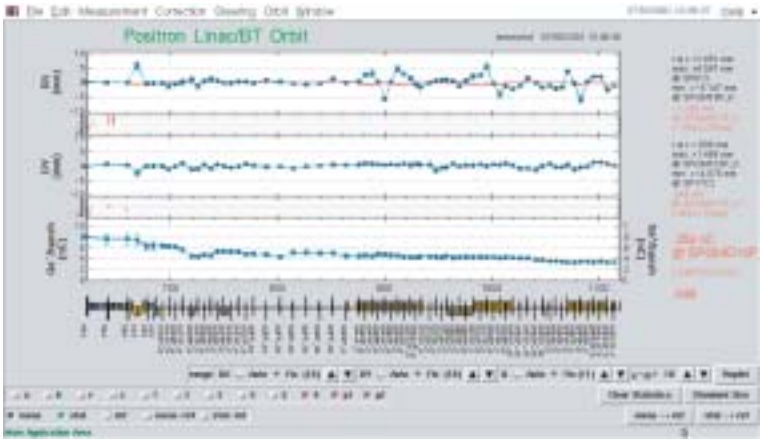

Fig. 7. Example of the beam orbit in the positron line.

injection. For monitoring the energy spread of the positron beam, we installed a wire scanner in the short arc before the long straight section, where the dispersion amounts to 3 m. Details are given elsewhere[1].

Three tungsten wires of 100 μm in diameter are strung on a frame for measuring the horizontal, vertical, and diagonal beam size. The frame moves along a line rotated by 45° to the horizontal plane, perpendicular to the beam direction. The stroke is 120 mm and the minimum step size is 4 μm. The vibration of the wire accompanied by the start and stop motion, which dominates the amplitude, was measured and found to be sufficiently small ($\pm 10\mu$m) compared to the beam size[4]. In the actual measurement we moved the wire in a "continuous mode"; the wire does not stop at the scheduled positions, but continuously moves, recording the signal coincident with the beam. In this mode we do not measure the wire position, but instead infer the position from the repetition rate of the beam and pulse counts of the stepping motor. This mode of operation greatly reduced the time necessary for a scan: 30 seconds for a scan.

We have mounted photomultiplier tubes (PMT) far downstream of the scanner to detect any gamma-ray coming from the wire due to the bremsstrahlung process. One PMT serves as gamma-ray monitors for two upstream scanners. Fig. 8 shows typical beam profiles measured with four wire scanners. The three peaks in each inset correspond to, from left to right, vertical, diagonal, and horizontal scan. Since we have no beam monitor that measures the positions or intensity of the beam in the pulse-to-pulse mode, no correction was made for the position jitter nor the intensity jitter of the beam.

Using the beam-size data at four wire positions, one can estimate the beta functions and the emittance at the most upstream wire based on an assumption that the beam has no correlation terms between the position and energy. The procedure of beta matching usually converges with a single iteration, with a criterion on convergence that the beta mismatch between the measured one

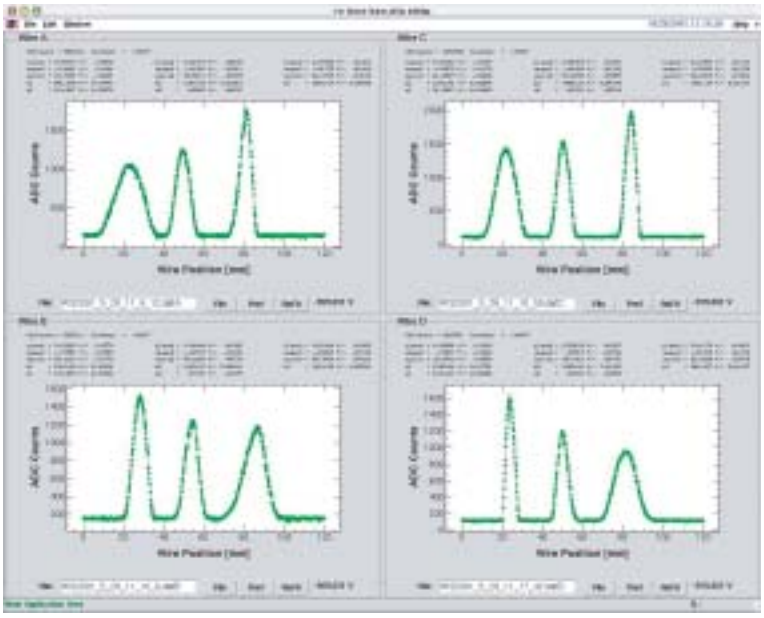

Fig. 8. Typical beam profiles in the positron line measured with four wire scanners.

and that of the design is less than 2, for example. Occasionally, however, it does not converge. In such a case, the incoming beam from the linac, itself, may have a dispersive correlation. Fig. 9 shows the variation in the optics parameters of the positron line for a period of twenty months operation. The horizontal parameters are displayed in the left figures while the vertical ones in the right. The bottom row shows the beta mismatch. In usual operation the optical parameters are measured once a day and optics matching is made if the beta-mismatch is greater than the criterion.

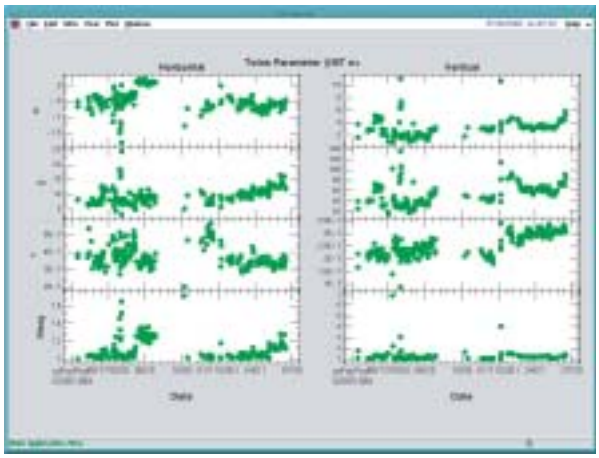

Fig. 9. Variation of the optics parameters in the positron line. The parameters in the horizontal plane are drawn in the left column while those in vertical planes are in the right. From top to bottom, the parameters of α, β, emittance, and beta mismatch are shown.

Besides wire scanners, 40 profile monitors and 23 beam-loss monitors utilizing

air-filled coaxial cables have been installed for the lines. The profile monitors have played a great role in checking the validity of the optics matching.

3 Injection system

Since the beam scattering in the window, even for Be, produces an enormous emittance increase, we adopted a scheme that does not utilize the injection window: the vacuum is common for the transport line and the ring. The dimensions of the beam chamber in the injection area of the ring are 65 mm in width, 48 mm in height for HER while 76 mm wide and 48 mm high for LER, which are maintained throughout the whole injection area in order to maintain smoothness. Four septum magnets for HER and two for LER are used for injection. They are all housed in vacuum chambers. Two septum chambers for HER and one septum chamber for LER, which are nearest to the ring, accommodate the beam chambers of the ring inside of them. The beam chamber of the ring is smoothly connected in the septum chambers, while keeping its inner dimension. The incoming beam is bent through the septum magnets and, after the quad, injected through a thin slit which is cut in the beam chamber of the ring. The gap height of the slit is 12 mm. A schematic injection orbit is shown in Fig. 10 for the HER case.

Since the total bend angle of septa is relatively large, 150 mrad for HER and 100 mrad for LER, an angle jitter of 0.1% gives rise to a sizable increase of the effective beam size. This means that the tolerance of each septum magnet must be less than .02%, which should be relatively tight for a pulsed magnet.

3.1 Injection septum

We adopted the "eddy current" type instead of the "current sheet" type, because it simplifies the electrical insulation of the coil, and also helps to make the septum thinner. In the "eddy current" type, on the other hand, the leak field outside of the septum is relatively large. In addition, it has a slow component that lasts even after the drive current has ceased. The leak field has a position dependence; it is smaller at longer distance from the septum. Since the position dependence of the slow component is much smaller than that of the fast component, the slow component exists even at the position of the circulating beam. We adopted an approach in which the slow component is partially canceled out by using a full-sine pulse, the positive swing being canceled with the succeeding negative swing. The leak field due to the eddy current is proportional to the pulse width. For a shorter pulse width, however, a higher voltage is needed, and it is more difficult to select a good power

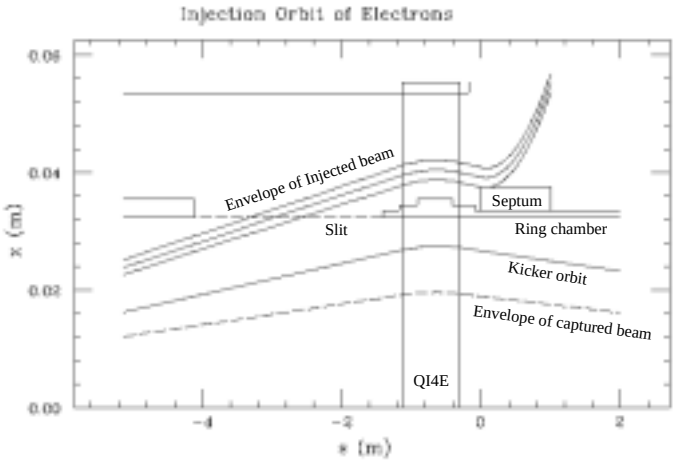

Fig. 10. Injection orbit of the electron beam. The vertical axis is the horizontal position from the beam center of HER, while the horizontal axis is the longitudinal position along the HER beam. The inner radius of the ring chamber is 32.5 mm. The beam is injected through a thin slit of the ring chamber, which is shown by a horizontal broken line. Also shown are the envelope of an injected beam of 2.5σ, the kicker orbit, and the envelope of a captured beam.

switch. As a compromise we adopted a pulse width of 280 μsec.

Table 2
Design parameters of the septum magnets.

		e^-	e^+
Deflection angle	(mrad)	37.5	50.0
Number of magnets		4	2
Peak magnetic field	(T)	1.04	0.79
Septum thickness	(mm)	2.5	2.5
Magnet core length	(m)	1.0	0.8
Magnet free aperture	(mm)	$11^H \times 44^W$	$11^H \times 44^W$
Laminate steel thickness	(mm)	0.1	0.1
Magnet inductance	(μH)	7.1	5.7
Peak current	(kA)	9.1	6.9
Peak voltage	(kV)	1.9	1.4
Voltage stability	(%)	0.02	0.02
Pulse width	(μsec)	280	260

3.1.1 magnet structure

The main parameters of the septum magnets are given in Table 2. The septum thickness in the table includes that of the shield plates. The magnet cores are made of 0.1 mm thick laminations stamped from silicon steel. The end plates are made of 15 mm thick stainless steel. The cores are surrounded by copper plates in order to reduce the leakage field. The coil is wound at the back-yoke by one turn and extracted outside of the chamber without any connection in the chamber. It makes use of a copper hollow-conductor, which has a coating of 0.3 mm thick ceramics to protect against voltage breakdown and radiation damage. In order to reduce any leakage field due to an eddy current in the copper septum, we attached two thin silicon steel plates of 0.5 mm thick outside the copper septum.

3.1.2 Power supplies and field measurements

The main capacitors are charged up precisely, with the voltage being controlled in precision by a deQing circuit at a fixed voltage level after the trigger. The capacitor is discharged by turning on six switch modules in parallel, each of which utilizes three thyristers in series; in a negative swing of the full-sine wave it is re-charged through a diode which is connected to the switch modules in parallel. The pulse height of the negative swing is 85% of the positive one, due to resistive loss in the coil and in the circuit. This reduction brings another imperfection in the cancellation of the leak field. Fig. 11 shows the current and voltage form. We have measured the magnetic field in various conditions. The

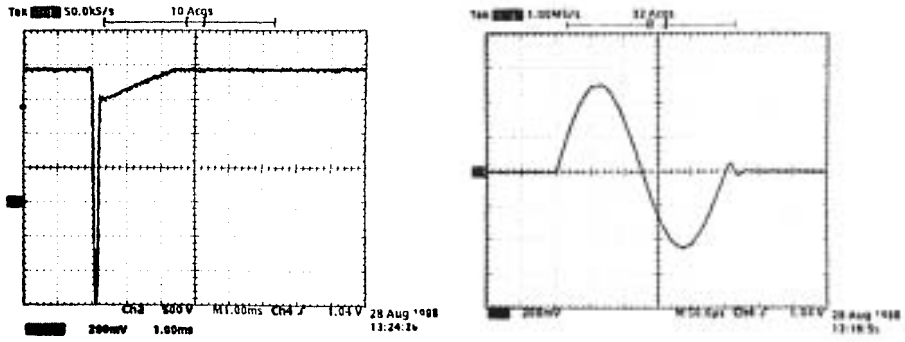

Fig. 11. Left: Voltage wave form, vertical scale 500V/div, horizontal scale 1ms/div, Right: Current wave form, vertical scale 4kA/div, horizontal scale 50μs/div

peak leak-field at a distance of 30 mm from the septum was 9 Gauss without a beam chamber. In this case the slow component of the leak field was 3% of the peak leak-field. In order to simulate the effect of the beam chamber we measured the leak field at the same place within an aluminum pipe of 2 mm thick and 20 mm diameter. The result was 2.5 Gauss. Since the real beam chamber has a much larger thickness, a much smaller leak field is expected in

the real configuration. We have achieved a voltage jitter of less than 0.02%, at least in short period of the observation time.

3.1.3 Operation status

The septum magnets have been successfully operated since December, 1998. The vacuum level in the septum chambers is, however, poor, though it has been improved slowly. This may become an issue in the future when the beam current will be increased. The high pressure in septum chambers is mainly due to out-gas from the silicon steel surface, which is coated with CrO_3 that includes an organic material as glue. When septum magnets are powered the temperature of the core is increased due to iron loss. Fig. 12 shows the temperature at various places of the septum magnets as well as the vacuum level in the septum chamber as a function of time during beam filling in HER, where the current was increased from 540 mA to 770 mA in 3.3 minutes. Fortunately,

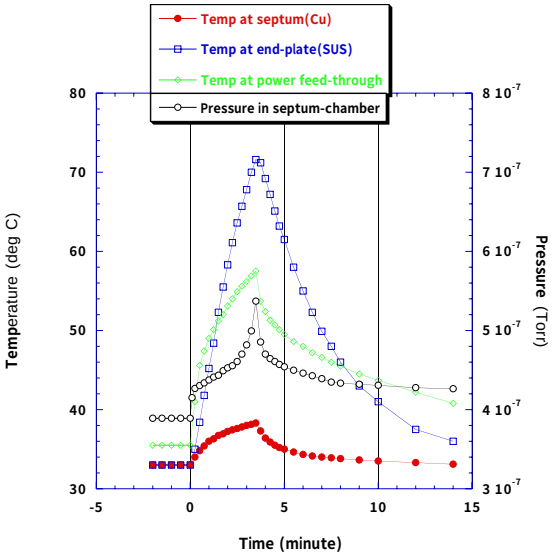

Fig. 12. Temperature of the magnet and the vacuum pressure. The septum was powered from 0 min to 3.3 min.

thanks to bad conductance between the septum chamber and the ring chamber, the poor vacuum has a relatively small effect on the vacuum in the ring. The abrupt increase in the vacuum pressure at the last minute of beam filling, seen in the Fig. 12, is also observed in the vacuum pressure in the ring. This phenomenon depends on the bunch current of the beam in the ring, and has a threshold. We suspect a HOM resonance near the septum. The vacuum pressure of the ring around the septa is roughly 5 to 10-times higher than those of the normal arc, while the pressure in the septum chamber is as high as 3 orders of magnitude. The outgassing rate of silicon steel that we used is comparable with that of rubber[5]. It might be necessary in higher current operation to

replace it with new steel that does not include any organic material in the coating.

3.2 Injection Kicker

The kicker bump orbit is generated by two groups of kickers whose horizontal phase difference is 180°. Each group consists of three kickers, i.e., six kickers are used in total for each ring. Single-turn injection needs 1.4 mrad and 2.8 mrad for a group of kickers for HER and LER, respectively. In usual multiple-turn injection we need 0.9 mrad and 1.8 mrad at maximum for HER and LER. Since the repetition rate is 50 Hz, which is comparable to a transverse damping time of 45 msec of the rings, a smaller pulse width compared to the revolution time of 10 μsec is necessary to make 50 Hz injection possible. We adopted a pulse width of 2 μsec.

3.2.1 Kicker magnets and power supplies

The kicker magnets are of the conventional window-frame type using a ferrite core. The ferrite core is 225 mm long and 90 mm high in the free gap. The kicker is mounted on a ceramic vacuum chamber. The maximum voltage and current of the power supply are 35 kV and 2000 A and the magnetic field is 550 Gauss. The voltage is low enough for stable operation of the thyratrons in the air. The shape of the current is a half sine (right bottom inset in Fig. 13). The same type of kicker magnet and the power supply are used for both rings. The stability of the peak current is less than 0.1%.

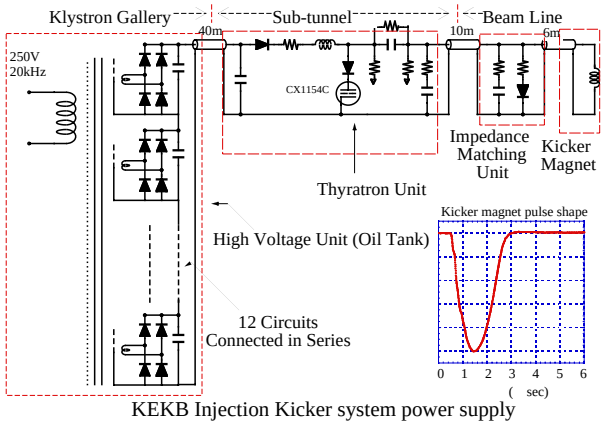

Fig. 13. Schematic diagram of the kicker-magnet system.

A deuterium-filled ceramic thyratron (CX1154C, Marconi Applied Technologies) was adopted as the power switch of the main circuit. Since many bunches exists in the time span of a kicker pulse it is important that the kicker orbit

bump is precisely closed; otherwise, the stored bunches would receive residual kicks, which would give rise to an adverse effect on the fast feedback system, for example. It is, thus, crucial to make the pulse shapes of kickers identical as well as to keep the phase advance of the two group of kickers 180°. Fig. 13 shows a simple circuit diagram of the power supply. By adjusting the resistor in the impedance match unit and also the stray inductance, we were able to control the pulse width and the undershoot depth.

3.2.2 Ceramic Chambers

We have developed novel water-cooled ceramic chambers[6] for HER and LER, as shown in Fig. 14. The length of the ceramic is 420 mm. Kovar was used as an intervening material between the ceramic and the SUS flange, since its thermal expansion matches that of the ceramic and eases the braze. From the

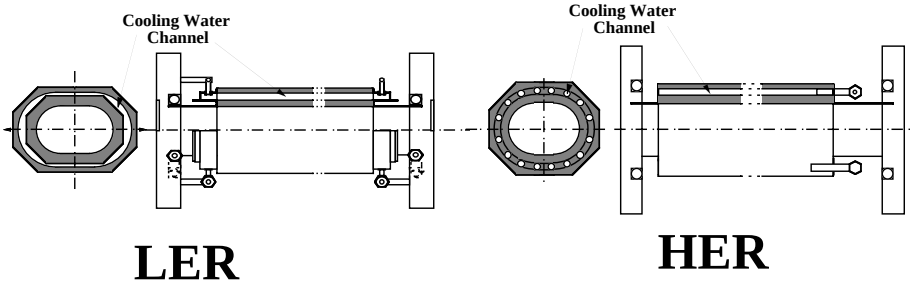

Fig. 14. Structure of the water-cooled ceramic chambers

view point of high-order mode loss, high-dimensional accuracy was required for the inner wall of the ceramic. It was ground so that the flatness of the inner surface would be less than 0.1 mm in 10 mm square area. At the junction of the ceramic and kovar, the step size was less than ± 0.2 mm.

The ceramic chamber for LER consists of two concentric chambers; in between them cooling water flows. It has fairly good cooling ability. Ti was adopted for braze metallization with an activated metallization method. The ceramic chamber for HER is, on the other hand, a single chamber which has 16 holes for cooling water drilled through the ceramic body. The water enters the chamber from upper and lower inlets, and after going back and forth twice it leaves from left and right water pipes. This type of ceramic chamber needs only one piece of ceramic, and is relatively easy to assemble. Since Mo-Mn is weak to water, though it is typically used for braze metallization of a ceramic, we adopted W-Mn.

A thin metallic coating is required on the inner wall to carry the beam image current and to confine the beam field in the beam chamber. The thickness of the coating should be, on the other hand, small enough so that the kicker field is not reduced too much due to an eddy current in the coating. The power from

the image current had been measured in the AR under a stored current of 500 mA. Extrapolating the data to the case of KEKB, it had been estimated to be approximately 1 kW for a 6μm Ti coating to the design current of 2.6 A. With this thickness, the power from eddy current was negligibly small, 20 to 50W, under a 50 Hz repetition rate. The inner surface was coated with Ti using Ti-Mn wire at the center of the chamber. The uniformity has been checked with a microscope for cut samples. Since the chamber shape is racetrack, the thickness was asymmetric; it was relatively thicker at the upper and lower sides and 60% thinner in the side arc.

3.2.3 Operation status

It was checked whether the kicker orbit bump is closed, making use of a single-pass beam position monitor of the fast-feedback system, which measures the beam position of each bunch on a turn-by-turn basis. Fig. 15 shows snapshots of the horizontal positions of each bunch around the injected bucket. Every

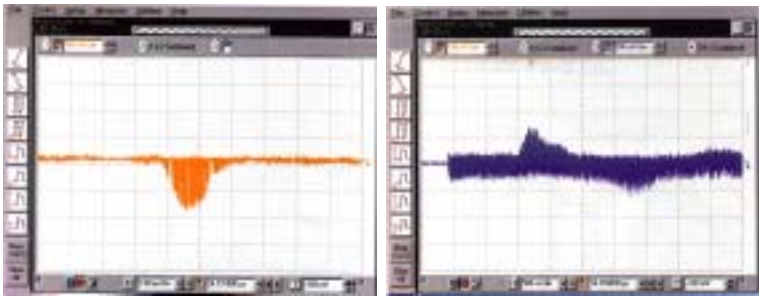

Fig. 15. Snapshots of the horizontal position of bunches around the injected-bucket. Left: pattern from kick angle error, 2 μs/div, Right: pattern from timing error, 0.5 μs/div

4th rf bucket was filled in this measurement. Since the location of the BPM is outside of the kicker orbit bump, no signal would be observed if the bump was closed. In the left figure of Fig. 15, the kick angle was different between the two groups of kickers. In this case, the shape of kicker pulse is imprinted on the pattern of bunch oscillation. By adjusting the kick angle, one can reduce the amplitude to a certain level, where, however, another type of pattern emerges, as shown in the right figure. Note that the vertical scale of the right figure is much smaller than that of the left. This pattern could be attributed to the time difference of the two kicker groups, and was able to be minimized by adjusting the trigger timing of the kicker magnets to some level that corresponds to 1.5% of the pulse shape distortion, or 10-30 μrad kick. The temperature rise at the ceramic surface was less than 1°C for a LER current of 950 mA and a HER current of 800 mA.

4 Beam abort system

The beam-abort system is an important element of KEKB for the protection of sensitive components of the Belle detectors and the accelerator components from damage due to intense beams. It is also indispensable for radiation safety. A beam-abort trigger is issued from many accelerator components as well as Belle when their parameters of, for example, temperature or radiation dose *etc.*, exceeds their threshold levels.

The beam-abort system is composed of two(one) horizontal kicker magnets, a vertical kicker, a Lambertson DC septum magnet and a beam dump for HER(LER). If one of the kickers fails to kick, an improperly deflected beam might hit some unexpected parts of the Belle or accelerator components and might give rise to irrecoverably serious damage. In order to avoid such risks, we adopted one common power supply for the kickers, where only one power switch is used.

4.1 Outline of the abort system

A schematic layout of the beam abort system of HER is shown in Fig. 16. Circulating beams are kicked horizontally with two horizontal kickers. The deflected beam, exiting the the ring through a thin Ti window of 1.4 mm thick, is bent downward by 100 mrad with the Lambertson DC septum magnet, and enters the beam dump. The beam traverses in air from downstream of the window. Power dissipation at the window due to the extracted beam is a

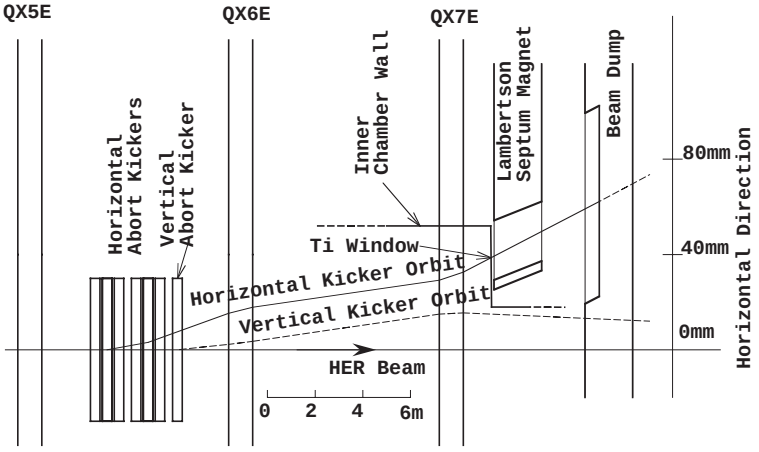

Fig. 16. Schematic layout of the abort system of HER

serious issue especially for LER. Since the beam size is very small, 500 μm in horizontal and 100 μm in vertical, for which we assume 3% coupling, the window would not bear the temperature rise. In order to relax the power

density at the window, we have used two tricks. Firstly, the vertical kicker, with a rise time greater than the revolution time, sweeps the beam in the vertical direction. The very small cross section of the beam in the vertical direction makes the vertical sweep effective in diffusing any heat deposit on the window. Secondly, we introduced an intentional ripple of $\pm 10\%$ at the flat top of the horizontal kicker pulse. Combining two dimensional deflections, the beam trajectory draws a serpentine pattern at the window, and the maximum power density is reduced by a factor of 5×10^{-3}. The maximum temperature of the window is estimated to be 660°C for a current of 2.6 A. We have not observed any hint of degradation in the window under the maximum current of 1 A.

The beam-abort systems have been working well since December, 1998. Now, both rings have an abort gap of 1μsec, or 10% of the circumference. This is required for the rise time of the horizontal kicker magnets. For higher luminosity, an improvement of the rise time of the horizontal kicker would be necessary.

4.2 Kicker magnets and power supply

The basic parameters of the kicker magnet are listed in Table 3. The horizontal

Table 3
Parameters of kicker magnets

		HER-H	HER-V	LER-H	LER-V
Deflection angle	(mrad)	1.875	1.2	1.93	1.4
Integrated field Bl	(T m)	.0525	.0336	.0238	.0173
Peak magnetic filed	(T)	.05	.0961	.0227	.0494
Peak current	(kA)	1.79	2.68	1.62	1.23
Number of turns		2	3	1	4
Inductance in design	(μH)	11.4	8.64	4.4	11.6
Gap height, width	(mm)	90, 160	105, 176	90, 160	125, 170
Ferrite Length	(mm)	900×2	300	900	300

kicker has three separated cores with a common coil, each having a separate ceramic chamber, because a single long ceramic chamber would be expensive and separate chambers would be beneficial when using the ceramic chamber developed for the injection kicker as a common part. Details of the ceramic chamber are found in section 3.2.

Fig. 17 shows a schematic diagram of the main part of the power supply for the HER, which supplies the pulse current simultaneously to the three kickers.

The power supply for LER has the same circuit with different parameters. The horizontal kickers are connected in parallel to make the rise time shorter. The

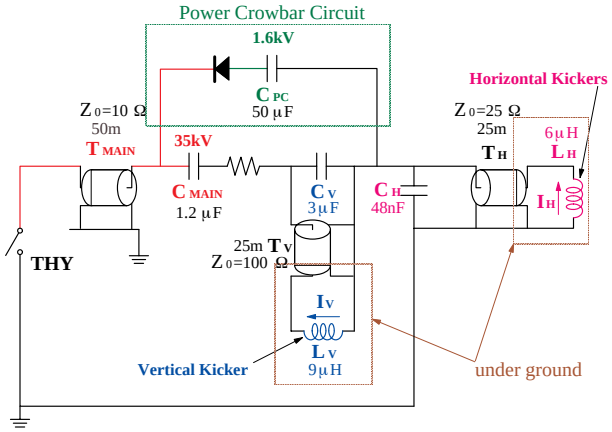

Fig. 17. Main circuit of power supply for the HER abort kickers. The charging circuits are not shown.

voltage (V_{MAIN}) of the main capacitance (C_{MAIN}) is 35 kV (19 kV) and the voltage of the capacitance (C_{PC}) is 1.6 kV (0.6 kV) for HER (LER). Charging circuits are not shown in the figure. We have used thyratrons as power switches, CX1175 and CX1154 (Marconi Applied Technologies), for HER and LER, respectively. Their maximum voltages are 70 kV and 40 kV, which give a large margin in voltage.

As the thyratron turns on, negative voltage pulse starts to travel through a cable (T_{MAIN}) 50 m long; when it reaches the other end, the voltage of the main capacitor (C_{MAIN}) jumps up to 70 kV, twice the charged voltage. This voltage continues for up to 500 nsec. The discharging current of C_{MAIN} starts to flow through mainly the coils of the horizontal kickers. Its rise time is determined by V_{MAIN} and the inductance of the horizontal kicker (L_H). The droop of the current (I_H) is compensated for by a discharge current of C_{PC}. On the other hand, the charge of C_V is resonantly discharged through the coil of the vertical kicker (L_V). From its resonant frequency, the rise time of the current (I_V) is determined to be $\sim 10\mu$sec. The ripples at the flat top of the horizontal kicker pulse are generated while making use of a resonant circuit composed of C_H and L_H. The period is about 3.3μsec. The amplitude of ripples is about $\pm 10\%$

4.3 Measurement of the magnetic fields

The integrated fields of kicker magnets along the beam direction in the ceramic chambers have been measured. Fig. 18 shows the results. The rise time of the horizontal field is about 1μsec and the ripples have sufficient amplitude during the time for a ring circumference of 10μsec. The field strength of the horizontal

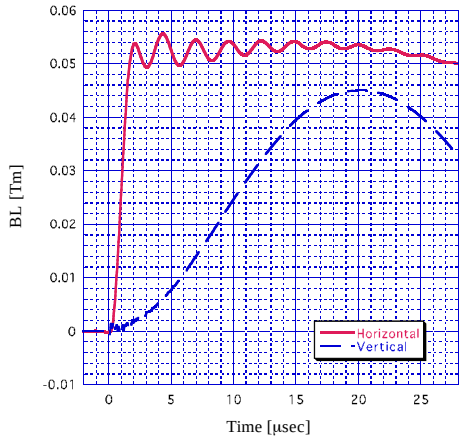

Fig. 18. Field strength of HER kicker magnet measured in the ceramic chamber

kicker satisfies the requirement in Table 3. The field strength of the vertical kicker at 10μsec is, however, 25% smaller than the value given in Table 3. To remedy this, we made the rise time faster by adjusting C_V, and also by adding a resistance to C_V in parallel. With these changes the field strength has satisfied the specifications.

5 Conclusion

We have constructed two beam lines from the injector linac to HER and LER of the KEKB, and also the injection system comprising the kickers and the eddy-current type septa. We have also implemented beam-abort systems for both rings. Specifically, we have developed novel water-cooled ceramic chambers for the kickers. These systems have been successfully operated since December, 1998.

Acknowledgments The authors appreciate the personnel of the KEKB group for their contributions to the construction of the present system, especially J. Flanagan for the beam-loss monitor, T. Suwada for profile monitors, N. Yamamoto for the control system, and S. Kurokawa for his help in magnet construction.

References

[1] N. Iida *et al.*, "Recent Progress of Wire Scanner Systems for the KEKB Injector Linac and Beam Transport Lines", Proc. of EPAC 2000, Vienna, Austria, pp1738-1740.

[2] T. Honda, M. Katoh, T. Mitsuhashi, A. Ueda, M. Tadano and Y. Kobayashi, J. Synchrotron Radiation 5 (1998) 618.

[3] T. Suwada, N. Kamikubota, H. Fukuma, N. Akasaka, and H. Kobayashi, Nucl. Instrum. Methods A440 (2000) 307.

[4] N. Iida *et al.*,"A Method for Measuring Vibrations in Wire Scanner Beam Profile Monitors", Proceedings of the APAC98, Tsukuba, Japan.

[5] Y. Satoh *et al.*, "Outgassing Measurement of the Laminated Cores for use of Pulse-operating Magnets", J. Vac. Soc. Jpn., vol. 43, No. 10, 2000, pp.24-28 (in Japanese)

[6] T. Mimashi *et al.*, "Water Cooling Ceramic Chamber for KEKB Kicker Magnet",Proceedings of the EPAC 2000, Vienna, Austria, June 2000, pp2444-2446.